ACS SyntheticBiology

pubs.acs.org/synthbio

Research Article

Cell-Free Protein Synthesis of Particulate Methane Monooxygenase into Nanodiscs

Christopher W. Koo, Jasmine M. Hershewe, Michael C. Jewett, and Amy C. Rosenzweig*

Cite This: *ACS Synth. Biol.* 2022, 11, 4009–4017

Read Online

ACCESS | Metrics & More | Article Recommendations | Supporting Information

ABSTRACT: Particulate methane monooxygenase (pMMO) is a multi-subunit membrane metalloenzyme used by methanotrophic bacteria to convert methane to methanol. A major hurdle to studying pMMO is the lack of a recombinant expression system, precluding investigation of individual residues by mutagenesis and hampering a complete understanding of its mechanism. Here, we developed an *Escherichia coli* lysate-based cell-free protein synthesis (CFPS) system that can be used to express pMMO in vitro in the presence of nanodiscs. We used a SUMO fusion construct to generate the native PmoB subunit and showed that the SUMO protease (Ulp1) cleaves the protein in the reaction mixture. Using an affinity tag to isolate the complete pMMO complex, we demonstrated that the complex forms without the need for exogenous translocon machinery or chaperones, confirmed by negative stain electron microscopy. This work demonstrates the potential for using CFPS to express multi-subunit membrane-bound metalloenzymes directly into lipid bilayers.

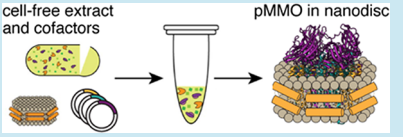

KEYWORDS: *cell free protein synthesis, membrane protein, copper, particulate methane monooxygenase, methanotroph*

INTRODUCTION

Emissions of methane, the second most important greenhouse gas after carbon dioxide, have been increasing rapidly over the past two decades.[1] Methane is a short-lived but potent greenhouse gas with 84 times the global warming potential of carbon dioxide over a 20 year period.[2] Thus, even modest reduction of methane emissions represents a near-term opportunity to fight rapid global warming.[3] Moreover, using excess methane to produce liquid fuel and value-added chemicals is highly desirable to meet rising energy demands.[4]

Methanotrophs, bacteria that metabolize methane as their sole carbon source, provide a promising biotechnological approach to these issues.[5,6] Found in a wide variety of environments, methanotrophs possess the unique ability to convert methane to methanol at ambient temperature and pressure.[7] In the first step of the aerobic methanotroph metabolic pathway, metalloenzymes called methane monooxygenases (MMOs) insert one atom of oxygen into the 105 kcal mol^{-1} C−H bond in methane. Methanotrophs can utilize two types of MMOs. An iron-dependent, soluble MMO (sMMO) is expressed under low copper conditions by some species,[8,9] and a copper-dependent membrane-bound or particulate MMO (pMMO) is produced by nearly all methanotrophs under copper-replete conditions.[10,11] While studies of sMMO have advanced to the level of trapping reaction intermediates,[12] identifying substrate pathways,[13] and characterizing the roles of regulatory subunits,[14] progress on pMMO has been comparatively slow due to the inherent difficulties in studying membrane proteins.[15] Multiple copper binding sites,[16−18] some involving strictly conserved amino acid residues, have been identified,[15] but the location of the active site and the roles of invariant residues have yet to be determined.

A major obstacle to addressing these questions is that there is currently no effective method to generate site-specific variants of pMMO. While mutagenesis can be performed in methanotrophs, all efforts to alter amino acids of likely functional importance have failed since pMMO is essential for cell survival.[15,19] A heterologous expression system is thus highly desirable, but recombinant overexpression of membrane proteins can be difficult due to misfolding, aggregation, disruption of the host's membrane environment, and subsequent suppression of gene expression by the host.[20−22] pMMO has the added challenges of requiring proper copper loading for enzymatic activity and being a multi-subunit complex formed from subunits PmoA (β), PmoB (α), and PmoC (γ), arranged in an $(\alpha\beta\gamma)_3$ trimer.[23,24] Indeed, only the primarily periplasmic PmoB subunit has been expressed successfully in *Escherichia coli*.[25,26] CRISPR-Cas9 gene editing has been reported for the methanotroph *Methylococcus capsulatus* (Bath)[27] but has not yet been demonstrated as useful for generating site-specific variants.

Cell-free protein synthesis (CFPS) offers an alternative strategy that addresses these difficulties.[28−30] *E. coli* lysate-based CFPS isolates the transcription and translation machinery from

Received: July 11, 2022
Published: November 23, 2022

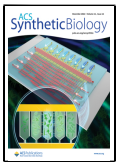

the cell, thus decoupling protein synthesis from normal cellular function and preventing inhibition or modification of an otherwise cytotoxic protein. The removal of the cell barrier creates an open, tunable reaction mixture that may be advantageous for membrane protein expression and can be modified to suit pMMO expression (Figure 1).[31−34] In particular, membrane mimetics such as liposomes, nanodiscs, bicelles, and detergents can be provided in the reaction, allowing direct expression into a membrane environment.[35−37] The CFPS system can also tolerate added copper for loading metalloenzymes[38] and provides a facile means of adding affinity tags to the individual pMMO subunits. Here, we have investigated the use of different membrane mimetics, fusion protein constructs of pMMO, and gene arrangements of the pMMO subunits in CFPS reactions, resulting in successful assembly of the pMMO trimer. This system represents the first CFPS-based expression of an assembled multi-subunit integral membrane metalloenzyme and underscores the potential of this approach for studying other difficult membrane protein complexes.

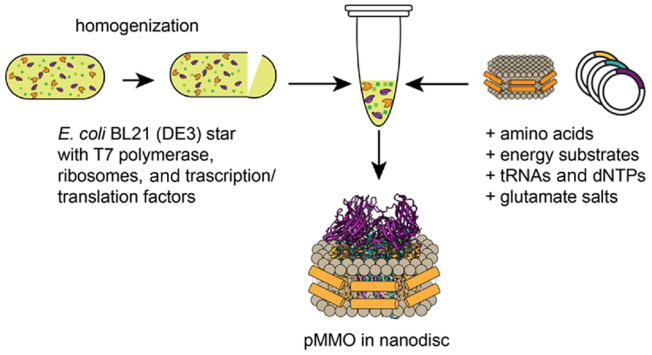

Figure 1. Schematic of pMMO cell-free expression reaction. The reaction components include transcription/translation factors from *E. coli*, plasmid DNA encoding pMMO, membrane mimetics such as nanodiscs, amino acids, tRNA, and dNTPs, and energy substrates such as phosphoenolpyruvate (PEP) and glutamate salts. The product of this reaction is the pMMO complex embedded in a lipid nanodisc.

RESULTS AND DISCUSSION

Initial Expression and Membrane Mimetic Test. We first tested the ability of different membrane mimetics to solubilize the pMMO subunits from *M. capsulatus* (Bath). Both nanodiscs and bicelles have been demonstrated to restore methane oxidation activity to inactive detergent-solubilized pMMO samples.[23,39] Bicelles are lipid bilayers that are solubilized by detergents, whereas nanodiscs are bilayers surrounded and rendered soluble by an amphipathic helical protein called a membrane scaffold protein (MSP). Nanodiscs are formed by solubilizing lipids and MSPs with detergent and subsequently removing the detergent, triggering the formation of stable nanodisc bilayers. Bicelles are less stable since they depend on a certain detergent-to-lipid ratio and concentration to maintain the bilayer, which will otherwise form liposomes if the detergent is diluted. The three pMMO subunits were expressed both individually and all together in the presence of 1 mg/mL POPC nanodiscs and 1% DMPC bicelles, concentrations that were used successfully to solubilize other membrane proteins in CFPS.[40−42] All three subunits show soluble expression in the presence of nanodiscs (Figure 2), indicating that the subunits can insert into the nanodiscs without any additional chaperones such as translocon machinery.[43,44] The use of bicelles reduced total expression by ∼25% and only resulted in minimal soluble expression (Figure 2). On the basis of these expression profiles, nanodiscs were used for further experiments.

SUMO Protease and Plasmid Ratios. The PmoB subunit includes a 32-residue N-terminal signal sequence that directs the soluble domain to the periplasm and is removed by an endogenous protease,[45] leaving His33 as the new N-terminal residue. The His33 amino group, along with its side chain imidazole group and those of residues His137 and His139, coordinates a copper ion (the Cu_B site).[17,23] To mimic signal peptide cleavage and ensure proper formation of the Cu_B site, an N-terminal SUMO-PmoB fusion protein was generated for processing by SUMO protease (Ulp1) (Figure 3A). Ulp1 protease has the advantage of cleaving at the C-terminus of the SUMO fusion protein, leaving no exogenous residues on the cleaved PmoB subunit.[46] To address the reduced expression of PmoB compared to the other two subunits (Figure 3C), the

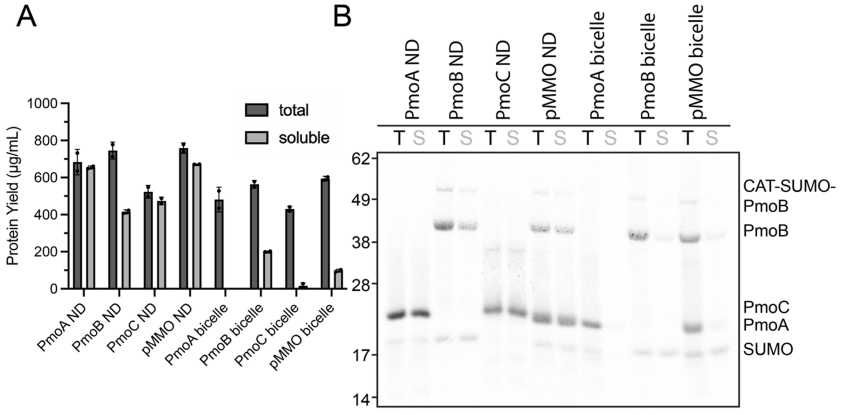

Figure 2. Cell-free expression of pMMO subunits using nanodiscs (ND) and bicelles. (A) Total and soluble expression of each subunit individually and all subunits in combination using bicelles or ND as a membrane mimetic, $n = 2$ replicates. (B) Autoradiogram of total (T) and soluble (S) expression for each reaction detecting protein bands labeled with ^{14}C-leucine. MW markers (SeeBlue prestained marker, Thermo Fisher Scientific) are positioned according to the equivalent SDS-PAGE gel. The PmoB subunit was expressed as a SUMO fusion protein to generate its native N-terminus (vide infra).

https://doi.org/10.1021/acssynbio.2c00366
ACS Synth. Biol. 2022, 11, 4009−4017

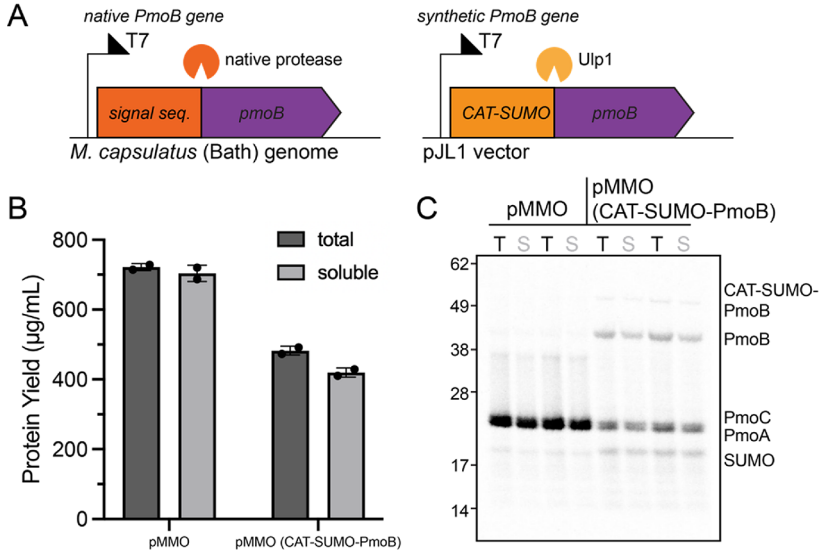

Figure 3. Cell-free expression of pMMO subunits using CAT-SUMO-PmoB. (A) Comparison of the native *pmoB* gene in the *M. capsulatus* (Bath) genome and the engineered gene used in this study. (B) Total and soluble expression of a mixture of plasmids expressing PmoA, PmoC, and either PmoB or CAT-SUMO-PmoB in nanodiscs (ND) as a membrane mimetic, $n = 2$ replicates. (C) Autoradiogram of total (T) and soluble (S) expression for each reaction detecting protein bands labeled with ^{14}C-leucine. MW markers (SeeBlue prestained marker, Thermo Fisher Scientific) are based on the equivalent SDS-PAGE gel (Figure S1).

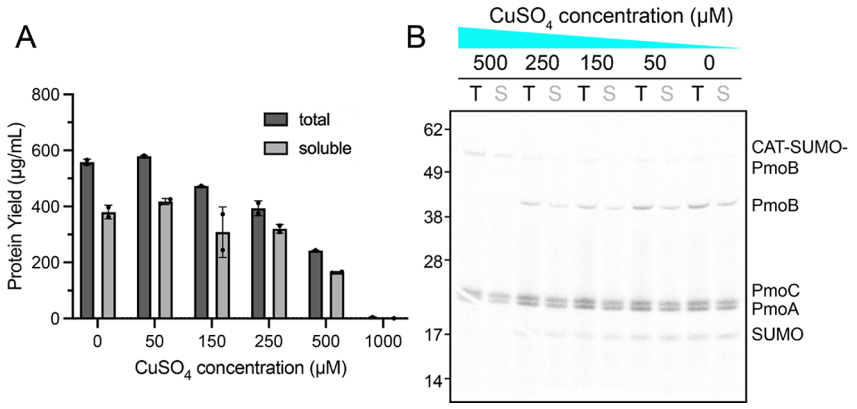

Figure 4. Copper sensitivity of pMMO CFPS reaction. (A) Total and soluble expression of pMMO with increasing amounts of $CuSO_4$, $n = 2$ replicates. (B) Autoradiogram showing the relative expression of pMMO subunits with increasing copper concentration. Molecular weights are marked according to the position of the SeeBlue (Thermo Fisher Scientific) markers (Figure S1).

sequence Met-Glu-Lys-Lys-Ile was added to the N-terminus of the SUMO tag[47,48] (Figure 3A). This sequence, derived from chloramphenicol acetyltransferase (CAT), is commonly used to enhance CFPS expression.[49] Cell-free reactions with plasmids for PmoA, PmoC, and CAT-SUMO-PmoB showed equimolar expression of the three subunits (Figure 3C). Furthermore, the SUMO tag was cleaved successfully in the reaction, generating the native N-terminus of PmoB.

Copper Tolerance. pMMO contains up to four copper binding sites,[17,23] and while the functional significance of each site is not fully established, a previous study has shown that copper is necessary to recover pMMO activity after metal removal.[18] Methanotrophs import copper for pMMO using several mechanisms, including secretion of copper-chelating natural products and proteins.[50] In the CFPS reaction, copper must be provided separately so the effect of added copper on expression of the pMMO subunits was investigated (Figure 4). Total protein expression begins to decrease with the inclusion of 150 μM $CuSO_4$, is reduced by ~50% at 500 μM $CuSO_4$, and is abolished at 1 mM $CuSO_4$. Soluble expression, however, is only modestly decreased at 250 μM $CuSO_4$, consistent with our previous work assessing copper tolerance for CFPS expression of a multicopper oxidase.[38] Therefore, 200 μM $CuSO_4$ was included in each subsequent reaction. Interestingly, SUMO cleavage was almost completely inhibited at 500 μM $CuSO_4$.

Multi-Versus Single-Plasmid Approach. In the *M. capsulatus* (Bath) genome, the pMMO subunit genes are organized in an operon as *pmoCAB* with a promoter identified upstream of *pmoC*. To replicate this arrangement, a single plasmid containing the genes in this order was designed. In an initial experiment, PmoC was expressed, but there was only a small amount of PmoA expression and no PmoB expression (Figure S2A). To improve expression of PmoA and PmoB, T7 promoters were added to each gene by switching from the pJL1 vector to the pCDF-Duet backbone with a third multiple cloning site included. In addition, the CAT sequence was appended to the PmoB N-terminus. This approach increased the expression of PmoB relative to PmoA and PmoC (Figure S2B). The CAT sequence was then added to the N-terminus of

https://doi.org/10.1021/acssynbio.2c00366
ACS Synth. Biol. 2022, 11, 4009−4017

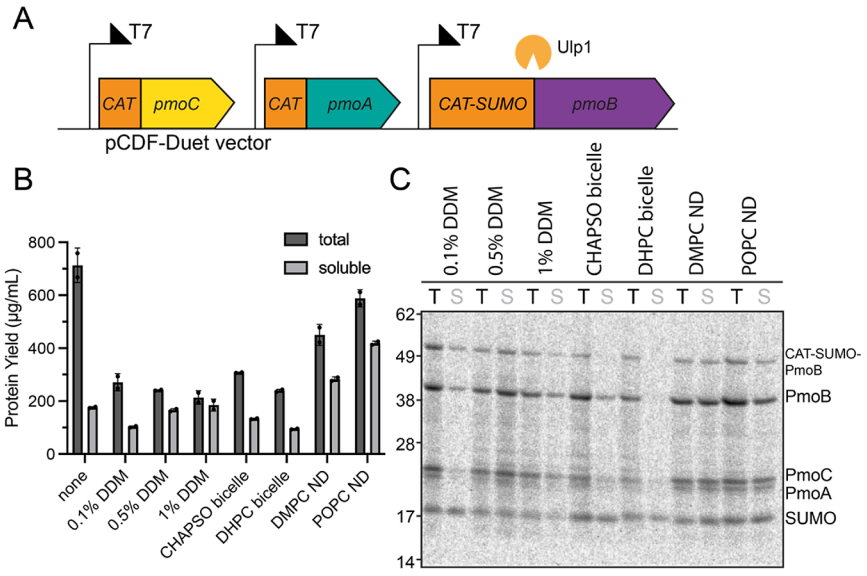

Figure 5. Polycistronic expression of pMMO and screen of membrane mimetics. (A) Arrangement of pMMO genes in the engineered pCDF-Duet vector, mimicking the native arrangement in the genome. (B) Total and soluble protein expression in detergent, bicelles, and nanodiscs, $n = 2$ replicates. DDM, *n*-dodecyl-*β*-D-maltoside (DDM); DHPC, 1,2-dihexanoyl-*sn*-glycero-3-phosphocholine; CHAPSO, 3-([3-cholamidopropyl]-dimethylammonio)-2-hydroxy-1-propanesulfonate; DMPC, 1,2-dimyristoyl-*sn*-glycero-3-phosphocholine; POPC, palmitoyl-2-oleoyl-*sn*-glycero-3-phosphocholine; ND, nanodisc. (C) Corresponding autoradiogram showing the relative expression of each pMMO subunit.

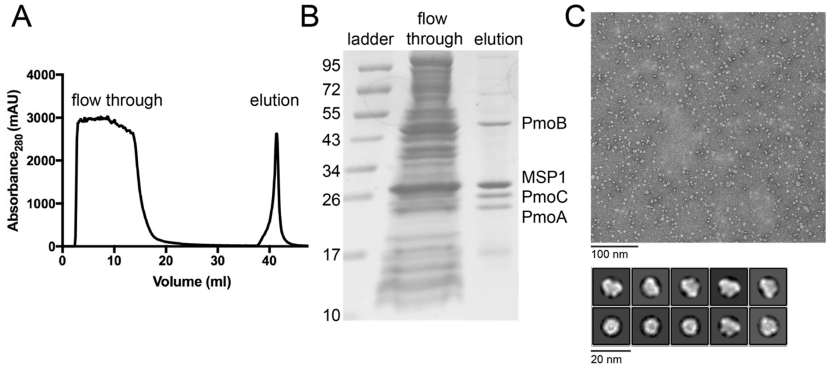

Figure 6. Isolation and negative stain EM of the pMMO complex produced by CFPS. (A) Purification profile on the StrepTactin Sepharose column (Cytiva). The pMMO complex was eluted using the Strep-tag II on the PmoC subunit. (B) SDS-PAGE gel showing the three pMMO subunits and the membrane scaffold protein MSP1E3D1 (MSP1) in the elution. (C) Representative negative stain micrograph and resulting 2D class averages.

all three genes (Figure 5A), and the resultant construct was tested using bicelles, different concentrations of detergent, and nanodiscs. Nanodiscs provided the best total and soluble expression of pMMO (Figure 5B) with expression of all three subunits and effective SUMO cleavage (Figure 5C). This optimized single-plasmid protocol was subsequently used for protein isolation.

Tagging Subunits and Isolation from CFPS. A major benefit of using CFPS for pMMO expression is the ability to add affinity tags to the subunits for purification. The C-termini of PmoA and PmoC face the cytoplasm and are relatively flexible,[24,51] providing promising sites for affinity tags. Adding a tag to the C-terminus of PmoB, which is periplasmic and folded into a beta sheet, might disrupt folding or complex assembly. However, since its N-terminus is unavailable due to the signal peptide and copper binding by His33, a C-terminal tag was tested for PmoB as well. The Strep-tag II and StrepTactin Sepharose beads (Cytiva) were used since this system results in less nonspecific binding and fewer contaminants from the affinity purification step. Reactions were scaled up from 30 to 500 μL for these tests and conducted in a sealed six-well culture plate rather than a 1.5 mL microfuge tube.[52] Analysis of the elution fractions from the affinity column showed that PmoC with a Strep-tag II pulled down the other two subunits and the nanodisc membrane scaffold protein, suggesting that the three subunits form a complex in a nanodisc (Figure 6A,B). The tagged PmoA and PmoB constructs failed to pull down the other subunits (Figure S3). This may be because the PmoA tag is inaccessible, and the PmoB Strep tag may disrupt folding or trimer formation. As such, the Strep-tag II PmoC construct was used for further experiments.

Functional Characterization. We next isolated the CFPS-produced pMMO complex with the goal of assessing activity. Unfortunately, the complex exhibited no methane oxidation activity, even with the addition of $CuSO_4$. The reaction mixture was tested for activity without purifying the complex but was found to have a high level of background methanol.

https://doi.org/10.1021/acssynbio.2c00366
ACS Synth. Biol. 2022, 11, 4009−4017

Although we use [^{13}C]methane in our activity assays, the 1% natural abundance of ^{13}C in the high level of background methanol confounds activity readings. Additionally, active pMMO from isolated methanotroph membranes was combined with the CFPS reaction mix to test the effects on activity. The reaction mix inhibits the activity of this membrane-bound pMMO, underscoring the need to purify the synthesized pMMO from the CFPS mix (Figure S4). Mixtures of the isolated complex with extract from *M. capsulatus* (Bath), possibly containing components missing in *E. coli*, were also found to be inactive. There may be cofactors that are essential for activity such as a partner protein or a small molecule metabolite that is present in methanotrophs, but not in the *E. coli* extract.

To identify possible reasons for the lack of activity and study the complex further, samples were prepared for negative stain and cryoelectron microscopy (cryo-EM). Polycistronic DNA was used in the presence of $CuSO_4$ and POPC nanodiscs, and the complex was purified using the Strep-tag II tag on the PmoC subunit (Figure 6A,B). Investigation of this sample by negative stain electron microscopy yielded 2D class average images of the pMMO complex that resemble native pMMO in a nanodisc[23] (Figure 6C). The trimeric structure is clearly present, providing further evidence that the full pMMO complex is expressed into a nanodisc in the cell-free reaction. Moreover, trimer formation necessitates proper folding of the three subunits. More subtle misfolding of specific regions, especially at the copper-binding sites, could account for the lack of activity, however.

CONCLUSIONS

In this work, we set out to demonstrate the synthesis of the pMMO complex in cell-free systems. To achieve this goal, we expressed pMMO subunits into an *E. coli*-based CFPS system enriched with nanodiscs. We showed how CFPS can be tuned and optimized to overcome the challenges of multi-subunit membrane complexes and copper metalloenzymes, along with how SUMO fusions can be used effectively in such reactions to increase reaction yields. Notably, negative-stain EM data showed that the pMMO complex assembles into a trimer similar to the native pMMO. While an important validation, we did not observe methane oxidation activity. pMMO expressed in living *E. coli* also does not show activity, hinting that factors essential for activity are lacking. Nevertheless, our work represents a first step to apply CFPS to investigate pMMO complexes in an open reaction mixture that allows for fine control over the environment and the construct being expressed. In the future, we expect that CFPS combined with membrane mimetic technology will become a powerful tool for investigating otherwise intractable membrane enzymes.

MATERIALS AND METHODS

Cloning and Construct Design. Codon-optimized constructs for the *pmoA*, *pmoB*, and *pmoC* genes from *M. capsulatus* (Bath) were synthesized (Genscript) and cloned individually into the pJL1 vector using Gibson assembly. These genes were also cloned into one pCDF-Duet vector backbone using both multiple cloning sites and creating a third site with its own promoter and ribosome binding site. The PmoC encoding gene included a C-terminal Strep-tag II sequence (Trp-Ser-His-Pro-Gln-Phe-Glu-Lys). PmoB was cloned with an N-terminal SUMO fusion protein.[46] The SUMO tag also had an N-terminal CAT sequence (Met-Glu-Lys-Lys-Ile), which has been shown to increase yield in the cell-free system.[47,48]

Cell-Free Extract Preparation. Cell growth was initiated by inoculating 5 mL LB cultures with BL21 Star (DE3) cells from a glycerol stock grown with no antibiotics overnight at 37 °C. This culture was used to inoculate a 100 mL LB culture, which was grown overnight at 37 °C. The 100 mL culture was then used to inoculate 1 L of 2xYT media with an initial optical density at 600 nm (OD_{600}) of 0.07. This culture was grown to an OD_{600} of 4.0 after ∼3 h at 37 °C and harvested by centrifugation at 8000*g* for 10 min at 4 °C, yielding approximately 10 g of cells. The cell pellet was washed in cold buffer containing 10 mM Tris-acetate, pH 8.2, 14 mM $Mg(acetate)_2$, and 60 mM potassium acetate by resuspending by vortexing followed by another round of centrifugation (repeated for a total of three washes). The cell pellet was weighed, flash-frozen in liquid nitrogen, and stored at −80 °C.

The cell extract was prepared by thawing the cell pellet in cold acetate buffer. Buffer was added to the pellet at a ratio of 0.8 mL per 1 g cells in a 50 mL conical tube followed by vortexing in 10 s increments, incubating the solution on ice in between vortexing to keep the cells as cold as possible. Once the cells were completely resuspended, the solution was lysed using a chilled Emulsiflex (ATA Scientific) by passing the solution through the system twice. The lysed cells were then centrifuged at 10,000*g* for 10 min at 4 °C to separate the insoluble cell material from the soluble cell extract. The soluble portion was collected, aliquoted, flash-frozen in liquid nitrogen, and stored at −80 °C.

Nanodisc Preparation. Membrane scaffold protein was prepared using established methods.[53,54] BL21 (DE3) cells containing the MSP1E3D1 plasmid (Addgene) were grown in TB media at 37 °C to an OD_{600} of 2.1, induced with 1 mM IPTG, grown for 4 h at 37 °C, and harvested by centrifugation at 8000*g* for 10 min. Cell pellets were weighed and flash-frozen in liquid nitrogen. To isolate MSP1E3D1, the pellet was resuspended in buffer containing 20 mM Tris, pH 8.0, 250 mM NaCl, and 10 mM imidazole and lysed by sonication for 10 min with 1/2 s on/off pulses on ice at 35% amplitude. The lysate was centrifuged at 20,000*g* for 30 min, and the soluble fraction was applied to a nickel-NTA gravity column. The beads were washed with 5 column volumes (cv) buffer containing 20 mM Tris, pH 8.0, 250 mM NaCl, 10 mM imidazole, and 50 mM sodium cholate followed by 10 cv buffer containing 20 mM Tris, pH 8.0, 250 mM NaCl, and 10 mM imidazole. MSP1E3D1 was eluted from the beads with 5 cv buffer containing 20 mM Tris, pH 8.0, 250 mM NaCl, and 250 mM imidazole. TEV protease was added at a ratio of 1:50 mol:mol, and the elution fraction was dialyzed against buffer containing 20 mM Tris, pH 8.0, 250 mM NaCl, and 10 mM imidazole overnight at 4 °C. This material was applied to nickel-NTA beads, and the flow through containing cleaved MSP1E3D1 was collected. The solution was concentrated and buffer-exchanged into 25 mM PIPES, pH 7.3, and 250 mM NaCl using an Amicon centrifugal concentrator with a 10 kDa molecular weight cutoff, aliquoted, and flash-frozen in liquid nitrogen.

POPC or DMPC lipids dissolved in chloroform were prepared by drying the solution under nitrogen until a thin layer was formed in a glass vial that was then dried overnight in a vacuum desiccator wrapped in foil. The lipids were resuspended to a concentration of 50 mM in buffer containing

https://doi.org/10.1021/acssynbio.2c00366
ACS Synth. Biol. 2022, 11, 4009−4017

25 mM PIPES, pH 7.3, 250 mM NaCl, and 100 mM sodium cholate by alternating vortexing, heating at 60 °C, and sonication in an ultrasonic bath until the lipids were fully dissolved. The lipid solution was aliquoted and stored at −20 °C.

Lipids and MSP1E3D1 were mixed together at molar ratios of 1:130 MSP1E3D1:POPC and 1:150 MSP1E3D1:DMPC. The mixture was mixed end over end at 20 rpm at 4 °C for 15 min and dialyzed against buffer containing 25 mM HEPES, pH 7.0, and 250 mM NaCl for 2 h at 4 °C, followed by buffer exchange and dialysis overnight. The solution was then concentrated and applied to a Superose 6 increase GL 10/300 column (Cytiva), and fractions containing empty nanodiscs were collected, aliquoted, and flash-frozen.

Cell-Free Reactions. Cell free reactions were prepared in either 30 μL reactions for radioactive quantitation tests in 1.5 mL microfuge tubes or 500 μL reactions for protein isolation in a six-well cell plate. The reaction mixture was composed of 8 mM magnesium glutamate, 10 mM ammonium glutamate, 130 mM potassium glutamate, 1.2 mM ATP, 0.85 mM each of UTP, CTP, and GTP, 0.034 mg/mL folic acid, 0.171 mg/mL *E. coli* tRNA mixture, 2 mM each of the 20 standard amino acids, 10 μM L-[^{14}C(U)]-leucine (only for radioactive quantitation experiments), 30 mM phosphoenolpyruvate (PEP), 0.33 mM nicotinamide adenine dinucleotide (NAD), 0.27 coenzyme-A (CoA), 4 mM sodium oxalate, 1 mM putrescine, 1.5 mM spermidine, 100 μg/mL T7 polymerase, 57 mM HEPES, pH 7.2, 26.7 μg/mL plasmid, 27% (v/v) extract, 50 μg/mL SUMO protease, 200 μM $CuSO_4$, and 1 mg/mL nanodiscs. All reactions were performed at room temperature for 20 h.[48,55,56]

Radioactive Quantification. Radioactive L-[^{14}C(U)]-leucine was added to 15 μL reactions for quantification of protein expression. At the end of the reaction, 2 μL was removed for gel electrophoresis and 4 μL was removed for quantification. The reaction was centrifuged at 12,000*g* for 10 min to pellet insoluble protein, 2 μL of the soluble fraction was removed for gel electrophoresis, and 4 μL was removed for quantification of soluble protein expression. NaOH (100 μL, 0.1 M) was added to each quantification fraction and incubated at 37 °C for 20 min. Two tabs of Whatman 3MM chromatography paper (GE Healthcare) were prepared for each reaction, marked "washed" and "unwashed", and suspended above an aluminum foil-wrapped Styrofoam block using straight pins. Following incubation, samples were mixed by pipetting and 50 μL was applied to each of the two filter papers and dried for 1 h under a heat lamp. Tabs designated for washing were placed in a beaker with 5% trichloroacetic acid (TCA) at 4 °C to precipitate the protein. After 15 min, the buffer was removed and replaced with fresh 5% TCA buffer, for a total of three exchanges. Afterward, the tabs were immersed in 100% ethanol for 10 min at room temperature. The tabs were then mounted on Styrofoam and dried for 1 h under a heat lamp. Finally, each tab was placed in a microfuge tube and submerged in 1 mL of scintillation fluid. The remaining radioactivity was measured using a MicroBeta 2 scintillation counter (Perkin Elmer). Protein yield was determined according to the following equation:

$$[((\text{washed cpm} - \text{background cpm})/\text{unwashed cpm}) \times [\text{leucine in rxn}]\ \mu\text{M} \times (\text{MW protein } \mu\text{g/mol})] /[(\text{number of leucine residues}) \times (1000\ \text{mL/L})] = \mu\text{g/mL}$$

Autoradiogram Analysis. For autoradiogram analysis, CFPS reactions included 10 μM L-[^{14}C(U)]-leucine. As described above, 2 μL each of the total and soluble fractions was collected and run on a 12% Bis-Tris NuPAGE gel (Thermo Fisher Scientific). After electrophoresis, the gel was soaked in gel drying solution (Bio-Rad) for 30 min and fixed with a cellophane film. The film was dried in a GelAir dryer (Bio-Rad) and exposed for 1 day on a Storage Phosphor screen (GE Healthcare). A Typhoon FLA 7000 imager (GE Healthcare) was then used to image the autoradiogram.

Protein Purification. The reaction mixture was centrifuged for 10 min at 14,000*g* and then applied to a 5 mL StrepTactin Sepharose column (Cytiva) followed by washing with 10 cv buffer containing 25 mM PIPES, pH 7.3, and 250 mM NaCl. The complex was eluted using 5 cv of the same buffer containing 2.5 mM desthiobiotin. Fractions containing the eluted complex were combined and concentrated using an Amicon filter (100 kDa MWCO, MilliporeSigma). The concentrated fractions were then applied to a Superose 6 increase 10/300 GL column (Cytiva), and peak fractions were collected and concentrated.

Activity Assays. The methane oxidation activity assay was conducted according to previously reported methods.[23,39] In each assay, 100 μL of pMMO was diluted to ∼1 mg mL^{-1} and mixed with excess reductant (duroquinol) in 2 mL glass screw-top vials with rubber septa (Agilent). Air (1 mL) was removed from the headspace, and 1.5 mL of [^{13}C]methane was added. The mixture was shaken at 45 °C at 200 rpm for 5 min followed by incubation on ice for 10 min. Negative controls were performed in the absence of [^{13}C]methane, duroquinol, or pMMO. In some assays, 1−5 equiv per pMMO protomer of $CuSO_4$ were added to the sample and incubated on ice for 2 h prior to the assay. In some assays, 75 μL of pMMO was mixed with 25 μL of the soluble extract (after cell debris and membrane removal) from *M. capsulatus* (Bath) to make the 100 μL sample. To test the effects of the CFPS reaction mixture on active pMMO, 50 μL of membranes with 10 mg/mL pMMO was added to 50 μL of the CFPS reaction mix to make a 100 μL sample. The activity of this sample was compared with that of 50 μL of the membranes mixed with 50 μL of buffer containing 25 mM PIPES, pH 7.3, and 250 mM NaCl.

Samples were prepared for GC−MS analysis by adding 500 μL of chloroform containing 1 mM dichloromethane to each sample. The samples were mixed at 4 °C at 2000 rpm for 10 min. The sample (2.5 μL) was then applied to a PoraBOND Q column (25 m × 250 μm × 3 μm) on an Agilent 7890B/5977A MSD GC/MS instrument with a 10:1 split ratio. The GC was maintained under a constant helium gas flow of 1.2 mL min^{-1}. The initial oven temperature was maintained at 80 °C for 3.5 min, increased at 50 °C min^{-1} to 150 °C, and held for 1.5 min. A second ramp rate of 15 °C min^{-1} was maintained up until a final temperature of 300 °C was reached and held there for 1 min. The mass spectrometer was maintained at 230 °C, quad temperature at 150 °C, 70 eV, and a detector voltage of 2999 V. Masses 31, 33, and 49 were

https://doi.org/10.1021/acssynbio.2c00366
ACS Synth. Biol. 2022, 11, 4009−4017

monitored for the detection of [^{12}C]methanol, [^{13}C]methanol, and dichloromethane, respectively. The [^{13}C]methanol peaks from standards were integrated, normalized to the concentration of dichloromethane, and quantified to form a standard curve. No peaks corresponding to [^{13}C]methanol were observed for the analyte samples.

Negative Stain Electron Microscopy and 2D Class Averaging. Carbon-coated copper grids (400 mesh, Thermo Fisher Scientific) were prepared for negative stain by applying 3 μL of the sample at 0.01 mg/mL and incubating at room temperature for 1 min. The sample was blotted using Whatman filter paper and washed in 50 μL drops of water for 15 s twice followed by 15 s in 50 μL drops of 2% uranyl formate twice. The grid was blotted, dried, and stored in a grid box. The sample was imaged using a JEM-1400 microscope (Jeol). Twelve images were collected with a random defocus ranging from 3 to 6 μm. The micrographs were analyzed using Relion v3.1.[57] Particles were picked using LoG picker with a range of 110−150 Å, resulting in 20,000 particles from which 2D class averages were generated.

■ ASSOCIATED CONTENT

Supporting Information

The Supporting Information is available free of charge at https://pubs.acs.org/doi/10.1021/acssynbio.2c00366.

Figures: (S1) examples of SDS-PAGE and autoradiogram side-by-side comparisons to obtain molecular weight (MW) marker positions, (S2) strategies for producing pMMO from a single plasmid, (S3) tagging pMMO subunits showing subunit assembly, and (S4) methane oxidation activity of isolated membranes containing pMMO in the presence and absence of CFPS mix (PDF)

■ AUTHOR INFORMATION

Corresponding Author

Amy C. Rosenzweig − *Department of Molecular Biosciences and of Chemistry and Center for Synthetic Biology, Northwestern University, Evanston, Illinois 60208, United States;* orcid.org/0000-0001-8472-4134; Email: amyr@northwestern.edu

Authors

Christopher W. Koo − *Department of Molecular Biosciences and of Chemistry, Northwestern University, Evanston, Illinois 60208, United States*

Jasmine M. Hershewe − *Department of Chemical and Biological Engineering, Northwestern University, Evanston, Illinois 60208, United States*

Michael C. Jewett − *Department of Chemical and Biological Engineering and Center for Synthetic Biology, Northwestern University, Evanston, Illinois 60208, United States;* orcid.org/0000-0003-2948-6211

Complete contact information is available at: https://pubs.acs.org/10.1021/acssynbio.2c00366

Author Contributions

All of the authors designed the research, C.W.K. and J.M.H. performed the research, A.C.R. and M.C.J. directed the research, and C.W.K., M.C.J., and A.C.R. wrote and edited the paper.

Notes

The authors declare the following competing financial interest(s): M.C.J. has a financial interest in SwiftScale Biologics, Gauntlet Bio, Pearl Bio, Inc., Design Pharmaceutics, and Stemloop Inc. M.C.J.'s interests are reviewed and managed by Northwestern University in accordance with their competing interest policies. All other authors declare no competing interests.

■ ACKNOWLEDGMENTS

This work was funded by National Institutes of Health grants R35GM118035 (A.C.R.) and T32GM008382 (C.W.K.), grant W52P1J-21-9-3023 from Army Contracting Command (M.C.J.), and Department of Energy grant DE-SC0018249 (M.C.J.). This work used resources of the Northwestern University Structural Biology Facility, which is generously supported by the NCI CCSG P30 CA060553 grant awarded to the Robert H. Lurie Comprehensive Cancer Center. We thank Andrew Hunt for providing the cell-free extract and for helpful discussions on running cell-free reactions.

■ REFERENCES

(1) Fletcher, S. E. M.; Schaefer, H. Rising methane: A new climate challenge. *Science* **2019**, *364*, 932−933.

(2) Kolstad, C.; Urama, K.*IPCC 2014 working group III contribution to the fifth assessment report of the intergovernmental panel on climate change*; Cambridge University: Cambridge, 2014.

(3) Stavert, A. R.; Saunois, M.; Canadell, J. G.; Poulter, B.; Jackson, R. B.; Regnier, P.; Lauerwald, R.; Raymond, P. A.; Allen, G. H.; Patra, P. K.; Bergamaschi, P.; Bousquet, P.; Chandra, N.; Ciais, P.; Gustafson, A.; Ishizawa, M.; Ito, A.; Kleinen, T.; Maksyutov, S.; McNorton, J.; Melton, J. R.; Muller, J.; Niwa, Y.; Peng, S.; Riley, W. J.; Segers, A.; Tian, H.; Tsuruta, A.; Yin, Y.; Zhang, Z.; Zheng, B.; Zhuang, Q. Regional trends and drivers of the global methane budget. *Global Change Biol.* **2022**, *28*, 182−200.

(4) Haynes, C. A.; Gonzalez, R. Rethinking biological activation of methane and conversion to liquid fuels. *Nat. Chem. Biol.* **2014**, *10*, 331−339.

(5) Hanson, R. S. Ecology and diversity of methylotrophic organisms. *Adv. Appl. Microbiol.* **1980**, *26*, 3−37.

(6) Semrau, J. D.; Dispirito, A. A.; Yoon, S. Methanotrophs and copper. *FEMS Microbiol. Lett.* **2010**, *34*, 496−531.

(7) Strong, P. J.; Xie, S.; Clarke, W. P. Methane as a resource: Can the methanotrophs add value? *Environ. Sci. Technol.* **2015**, *49*, 4001−4018.

(8) Ross, M. O.; Rosenzweig, A. C. A tale of two methane monooxygenases. *J. Biol. Inorg. Chem.* **2017**, *22*, 307−319.

(9) Banerjee, R.; Jones, J. C.; Lipscomb, J. D. Soluble methane monooxygenase. *Annu. Rev. Biochem.* **2019**, *88*, 409−431.

(10) Koo, C. W.; Rosenzweig, A. C., Particulate methane monooxygenase and the PmoD protein. In *Encyclopedia of Inorganic and Bioinorganic Chemistry*;Scott, R. A., Ed. John Wiley & Sons, Ltd: 2020.

(11) Sirajuddin, S.; Rosenzweig, A. C. Enzymatic oxidation of methane. *Biochemistry* **2015**, *54*, 2283−2294.

(12) Castillo, R. G.; Banerjee, R.; Allpress, C. J.; Rohde, G. T.; Bill, E.; Que, L.; Lipscomb, J. D.; DeBeer, S. High-energy-resolution fluorescence-detected X-ray absorption of the Q intermediate of soluble methane monooxygenase. *J. Am. Chem. Soc.* **2017**, *139*, 18024−18033.

(13) Jones, J. C.; Banerjee, R.; Shi, K.; Aihara, H.; Lipscomb, J. D. Structural studies of *Methylosinus trichosporium* OB3b soluble methane monooxygenase hydroxylase and regulatory component complex reveal a transient substrate tunnel. *Biochemistry* **2020**, *59*, 2946−2961.

(14) Srinivas, V.; Banerjee, R.; Lebrette, H.; Jones, J. C.; Aurelius, O.; Kim, I. S.; Pham, C. C.; Gul, S.; Sutherlin, K.; Bhowmick, A.;

John, J.; Bozkurt, E.; Fransson, T.; Aller, P.; Butryn, A.; Bogacz, I.; Simon, P. S.; Keable, S.; Britz, A.; Tono, K.; Kim, K. S.; Park, S. Y.; Lee, S. J.; Park, J.; Alonso-Mori, R.; Fuller, F.; Batyuk, A.; Brewster, A.; Bergmann, U.; Sauter, N.; Orville, A. M.; Yachandra, V. K.; Yano, J.; Lipscomb, J. D.; Kern, J. F.; Högbom, M. High resolution XFEL structure of the soluble methane monooxygenase hydroxylase complex with its regulatory component at ambient temperature in two oxidation states. *J. Am. Chem. Soc.* **2020**, *142*, 14249−14266.

(15) Koo, C. W.; Rosenzweig, A. C. Biochemistry of aerobic biological methane oxidation. *Chem. Soc. Rev.* **2021**, *50*, 3424−3436.

(16) Jodts, R. J.; Ross, M. O.; Koo, C. W.; Doan, P. E.; Rosenzweig, A. C.; Hoffman, B. H. Coordination of the copper centers in particulate methane monooxygenase: Comparison between methanotrophs and characterization of the Cu_C site by EPR and ENDOR spectroscopies. *J. Am. Chem. Soc.* **2021**, *143*, 15358−15368.

(17) Ross, M. O.; MacMillan, F.; Wang, J.; Nisthal, A.; Lawton, T. J.; Olafson, B. D.; Mayo, S. L.; Rosenzweig, A. C.; Hoffman, B. M. Particulate methane monooxygenase contains only mononuclear copper centers. *Science* **2019**, *364*, 566−570.

(18) Sirajuddin, S.; Barupala, D.; Helling, S.; Marcus, K.; Stemmler, T. L.; Rosenzweig, A. C. Effects of zinc on particulate methane monooxygenase activity and structure. *J. Biol. Chem.* **2014**, *289*, 21782−21794.

(19) Ro, S. Y.; Schachner, L. F.; Koo, C. W.; Purohit, R.; Remis, J. P.; Kenney, G. E.; Liauw, B. W.; Thomas, P. M.; Patrie, S. M.; Kelleher, N. L.; Rosenzweig, A. C. Native top-down mass spectrometry provides insights into the copper centers of membrane-bound methane monooxygenase. *Nat. Commun.* **2019**, *10*, 2675.

(20) Klepsch, M. M.; Persson, J. O.; de Gier, J.-W. Consequences of the overexpression of a eukaryotic membrane protein, the human KDEL receptor, in *Escherichia coli*. *J. Mol. Biol.* **2011**, *407*, 532−542.

(21) Bill, R. M.; Henderson, P. J. F.; Iwata, S.; Kunji, E. R. S.; Michel, H.; Neutze, R.; Newstead, S.; Poolman, B.; Tate, C. G.; Vogel, H. Overcoming barriers to membrane protein structure determination. *Nat. Biotechnol.* **2011**, *29*, 335−340.

(22) Pandey, A.; Shin, K.; Patterson, R. E.; Liu, X. Q.; Rainey, J. K. Current strategies for protein production and purification enabling membrane protein structural biology. *Biochem. Cell Biol.* **2016**, *94*, 507−527.

(23) Koo, C. W.; Tucci, F. J.; He, Y.; Rosenzweig, A. C. Recovery of particulate methane monooxygenase structure and activity in a lipid bilayer. *Science* **2022**, *375*, 1287−1291.

(24) Lieberman, R. L.; Rosenzweig, A. C. Crystal structure of a membrane-bound metalloenzyme that catalyses the biological oxidation of methane. *Nature* **2005**, *434*, 177−182.

(25) Kim, H. J.; Huh, J.; Kwon, Y. W.; Park, D.; Yu, Y.; Jang, Y. E.; Lee, B.-R.; Jo, E.; Lee, E. J.; Heo, Y.; Lee, W.; Lee, J. Biological conversion of methane to methanol through genetic reassembly of native catalytic domains. *Nat. Catal.* **2019**, *2*, 342−353.

(26) Balasubramanian, R.; Smith, S. M.; Rawat, S.; Yatsunyk, L. A.; Stemmler, T. L.; Rosenzweig, A. C. Oxidation of methane by a biological dicopper centre. *Nature* **2010**, *465*, 115−119.

(27) Tapscott, T.; Guarnieri, M. T.; Henard, C. A. Development of a CRISPR/Cas9 system for *Methylococcus capsulatus* in vivo gene editing. *Appl. Environ. Microbiol.* **2019**, *85*, No. e00340.

(28) Silverman, A. D.; Karim, A. S.; Jewett, M. C. Cell-free gene expression: An expanded repertoire of applications. *Nat. Rev. Genet.* **2020**, *21*, 151−170.

(29) Carlson, E. D.; Gan, R.; Hodgman, C. E.; Jewett, M. C. Cell-free protein synthesis: Applications come of age. *Biotechnol. Adv.* **2012**, *30*, 1185−1194.

(30) Perez, J. G.; Stark, J. C.; Jewett, M. C. Cell-free synthetic biology: Engineering beyond the cell. *Cold Spring Harbor Perspect. Biol.* **2016**, *8*, a023853.

(31) Karyolaimos, A.; Ampah-Korsah, H.; Zhang, Z.; de Gier, J. W. Shaping *Escherichia coli* for recombinant membrane protein production. *FEMS Microbiol. Lett.* **2018**, *365*, fny152.

(32) Hershewe, J. M.; Warfel, K. F.; Iyer, S. M.; Peruzzi, J. A.; Sullivan, C. J.; Roth, E. W.; DeLisa, M. P.; Kamat, N. P.; Jewett, M. C. Improving cell-free glycoprotein synthesis by characterizing and enriching native membrane vesicles. *Nat. Commun.* **2021**, *12*, 2363.

(33) Schoborg, J. A.; Hershewe, J. M.; Stark, J. C.; Kightlinger, W.; Kath, J. E.; Jaroentomeechai, T.; Natarajan, A.; DeLisa, M. P.; Jewett, M. C. A cell-free platform for rapid synthesis and testing of active oligosaccharyltransferases. *Biotechnol. Bioeng.* **2018**, *115*, 739−750.

(34) Matthies, D.; Haberstock, S.; Joos, F.; Dotsch, V.; Vonck, J.; Bernhard, F.; Meier, T. Cell-free expression and assembly of ATP synthase. *J. Mol. Biol.* **2011**, *413*, 593−603.

(35) Sachse, R.; Dondapati, S. K.; Fenz, S. F.; Schmidt, T.; Kubick, S. Membrane protein synthesis in cell-free systems: From bio-mimetic systems to bio-membranes. *FEBS Lett.* **2014**, *588*, 2774−2781.

(36) Klammt, C.; Schwarz, D.; Lohr, F.; Schneider, B.; Dotsch, V.; Bernhard, F. Cell-free expression as an emerging technique for the large scale production of integral membrane protein. *FEBS J.* **2006**, *273*, 4141−4153.

(37) Henrich, E.; Hein, C.; Dötsch, V.; Bernhard, F. Membrane protein production in *Escherichia coli* cell-free lysates. *FEBS Lett.* **2015**, *589*, 1713−1722.

(38) Li, J.; Lawton, T. J.; Kostecki, J. S.; Nisthal, A.; Fang, J.; Mayo, S. L.; Rosenzweig, A. C.; Jewett, M. C. Cell-free protein synthesis enables high yielding synthesis of an active multicopper oxidase. *Biotechnol. J.* **2016**, *11*, 212−218.

(39) Ro, S. Y.; Ross, M. O.; Deng, Y. W.; Batelu, S.; Lawton, T. J.; Hurley, J. D.; Stemmler, T. L.; Hoffman, B. M.; Rosenzweig, A. C. From micelles to bicelles: Effect of the membrane on particulate methane monooxygenase activity. *J. Biol. Chem.* **2018**, *293*, 10457−10465.

(40) Lyukmanova, E. N.; Shenkarev, Z. O.; Khabibullina, N. F.; Kopeina, G. S.; Shulepko, M. A.; Paramonov, A. S.; Mineev, K. S.; Tikhonov, R. V.; Shingarova, L. N.; Petrovskaya, L. E.; Dolgikh, D. A.; Arseniev, A. S.; Kirpichnikov, M. P. Lipid-protein nanodiscs for cell-free production of integral membrane proteins in a soluble and folded state: Comparison with detergent micelles, bicelles and liposomes. *Biochim. Biophys. Acta* **1818**, *2012*, 349−358.

(41) Hein, C.; Henrich, E.; Orban, E.; Dotsch, V.; Bernhard, F. Hydrophobic supplements in cell-free systems: Designing artificial environments for membrane proteins. *Eng. Life Sci.* **2014**, *14*, 365−379.

(42) Uhlemann, E.-M. E.; Pierson, H. E.; Fillingame, R. H.; Dmitriev, O. Y. Cell-free synthesis of membrane subunits of ATP synthase in phospholipid bicelles: NMR shows subunit *a* fold similar to the protein in the cell membrane. *Protein Sci.* **2012**, *21*, 279−288.

(43) Baumann, A.; Kerruth, S.; Fitter, J.; Buldt, G.; Heberle, J.; Schlesinger, R.; Ataka, K. In-situ observation of membrane protein folding during cell-free expression. *PLoS One* **2016**, *11*, e0151051.

(44) Hovijitra, N. T.; Wuu, J. J.; Peaker, B.; Swartz, J. R. Cell-free synthesis of functional aquaporin Z in synthetic liposomes. *Biotechnol. Bioeng.* **2009**, *104*, 40−49.

(45) Semrau, J. D.; Chistoserdov, A.; Lebron, J.; Costello, A.; Davagnino, J.; Kenna, E.; Holmes, A. J.; Finch, R.; Murrell, J. C.; Lidstrom, M. E. Particulate methane monooxygenase genes in methanotrophs. *J. Bacteriol.* **1995**, *177*, 3071−3079.

(46) Lawton, T. J.; Kenney, G. E.; Hurley, J. D.; Rosenzweig, A. C. The CopC family: Structural and bioinformatic insights into a diverse group of periplasmic copper binding proteins. *Biochemistry* **2016**, *55*, 2278−2290.

(47) Dudley, Q. M.; Nash, C. J.; Jewett, M. C. Cell-free biosynthesis of limonene using enzyme-enriched *Escherichia coli* lysates. *Synth. Biol* **2019**, *4*, ysz003.

(48) Jewett, M. C.; Swartz, J. R. Mimicking the *Escherichia coli* cytoplasmic environment activates long-lived and efficient cell-free protein synthesis. *Biotechnol. Bioeng.* **2004**, *86*, 19−26.

(49) Martin, R. W.; Des Soye, B. J.; Kwon, Y. C.; Kay, J.; Davis, R. G.; Thomas, P. M.; Majewska, N. I.; Chen, C. X.; Marcum, R. D.; Weiss, M. G.; Stoddart, A. E.; Amiram, M.; Ranji Charna, A. K.; Patel, J. R.; Isaacs, F. J.; Kelleher, N. L.; Hong, S. H.; Jewett, M. C. Cell-free

https://doi.org/10.1021/acssynbio.2c00366
ACS Synth. Biol. 2022, 11, 4009−4017

protein synthesis from genomically recoded bacteria enables multisite incorporation of noncanonical amino acids. *Nat. Commun.* **2018**, *9*, 1203.
(50) Kenney, G. E.; Rosenzweig, A. C. Methanobactins: Maintaining copper homeostasis in methanotrophs and beyond. *J. Biol. Chem.* **2018**, *293*, 4606−4615.
(51) Smith, S. M.; Rawat, S.; Telser, J.; Hoffman, B. M.; Stemmler, T. L.; Rosenzweig, A. C. Crystal structure and characterization of particulate methane monooxygenase from *Methylocystis* species strain M. *Biochemistry* **2011**, *50*, 10231−10240.
(52) Voloshin, A. M.; Swartz, J. R. Efficient and scalable method for scaling up cell free protein synthesis in batch mode. *Biotechnol. Bioeng.* **2005**, *91*, 516−521.
(53) McLean, M. A.; Gregory, M. C.; Sligar, S. G. Nanodiscs: A controlled bilayer surface for the study of membrane proteins. *Annu. Rev. Biophys.* **2018**, *47*, 107−124.
(54) Bayburt, T. H.; Sligar, S. G. Membrane protein assembly into nanodiscs. *FEBS Lett.* **2010**, *584*, 1721−1727.
(55) Jewett, M. C.; Calhoun, K. A.; Voloshin, A.; Wuu, J. J.; Swartz, J. R. An integrated cell-free metabolic platform for protein production and synthetic biology. *Mol. Syst. Biol.* **2008**, *4*, 220.
(56) Kwon, Y. C.; Jewett, M. C. High-throughput preparation methods of crude extract for robust cell-free protein synthesis. *Sci. Rep.* **2015**, *5*, 8663.
(57) Zivanov, J.; Nakane, T.; Forsberg, B. O.; Kimanius, D.; Hagen, W. J.; Lindahl, E.; Scheres, S. H. New tools for automated high-resolution cryo-EM structure determination in RELION-3. *eLife* **2018**, *7*, No. e42166.

https://doi.org/10.1021/acssynbio.2c00366
ACS Synth. Biol. 2022, 11, 4009−4017